Available online at www.sciencedirect.com
ScienceDirect
Comput. Methods Appl. Mech. Engrg. 293 (2015) 114–130
Computer methods in applied mechanics and engineering
www.elsevier.com/locate/cma

Implicit finite element formulation of multiresolution continuum theory

Hao Qin[a,*], Lars-Erik Lindgren[a], Wing Kam Liu[b], Jacob Smith[b]

[a] *Luleå University of Technology, Porsön, 971 87 Luleå, Sweden*
[b] *Northwestern University, Evanston, USA*

Received 6 June 2014; received in revised form 14 April 2015; accepted 27 April 2015
Available online 6 May 2015

Highlights

- The implementation of an implicit MRCT element into FEAP has been verified.
- Second order convergence in the equilibrium iterations is obtained.
- Mesh independent results in the case of deformation localization can be obtained.
- The element gives no dynamics for quasistatic cases in contrast to the explicit version.

Abstract

The multiresolution continuum theory is a higher order continuum theory where additional kinematic variables account for microstructural inhomogeneities at several distinct length scales. This can be particularly important for localization problems. The strength of this theory is that it can account for details in the microstructure of a material without using an extremely fine mesh. The present paper describes the implementation and verification of a 3D elastic–plastic multiresolution element based on an implicit time stepping algorithm. It is implemented in the general purpose finite element program FEAP. The mesh independency associated with the length scale parameter is examined and the convergence rate of the element is also evaluated.

Keywords: Multiresolution continuum theory; Finite element method; Damage; Localization

1. Introduction

The Multiresolution Continuum Theory (MRCT) developed by Liu and his coworkers [1] has been applied to study the void nucleation, growth and coalescence for steels [2–4] and a WC-Co composite [3,5]. The zig-zag ductile fracture profile has also been captured by a hybrid multiresolution approach detailed in [6]. The aforementioned studies using MRCT have been conducted using explicit time integration exclusively. The current paper focuses on numerical issues such as the implementation and verification of an implicit formulation of a 3D MRCT element into

* Corresponding author. Tel.: +46 076 777 2188.
E-mail addresses: hao.qin@ltu.se (H. Qin), lel@ltu.se (L.-E. Lindgren), w-liu@northwestern.edu (W.K. Liu).

http://dx.doi.org/10.1016/j.cma.2015.04.009
0045-7825/

FEAP [7]. We investigate particularly the utilization of the embedded length scale to converge to mesh independent solution. The aim of our work is to use the MRCT element to simulate necking and fracturing processes where the implicit method can be a better choice than the explicit MRCT element.

2. Microstructure, material properties and length scale

The response of a material to various load conditions depends on its structure. This structure, being largely hierarchical, is primarily dictated by its chemical composition and thermo-mechanical history. In traditional finite element methods, the description of the deformation and failure of a material is based on the assumption that the material is homogeneous over the volume represented by an integration point within an element. The size of the element used is typically much larger when compared to any microstructural component within the material. Therefore, homogenized constitutive models are calibrated using test specimens with dimensions that far exceed those characteristics of the scales of the microstructure.

Homogenization theory [8–10] is generally based on the concept of a representative volume element (RVE) of the underlying microstructure. Homogenization occurs when the mechanical responses resulting from a multifarious selection of loading conditions applied to the heterogeneous RVE are averaged. The finite element representation of this RVE consists of stresses, strains, and internal state variables evaluated at a material point. The relations between these variables depend only on their local values, previous history of deformation and temperature. The traditional homogenization approach often works well for hardening behavior, however, as damage and subsequent fracture are a weakest link approach, the details at the scale of the microstructure becomes increasingly important in modeling these phenomena if sufficient accuracy is to be achieved. Furthermore, softening leads to a localization of the deformation to the smallest element in the model, thus, the predicted results are highly mesh dependent.

Strain gradient theory was first introduced by the Cosserat brothers [11] and were further developed, e.g. [12–15], in order to remove the notorious mesh dependency for localization problems. Theories established in this category inherently include size effects in the constitutive equations. The multiresolution continuum theory (MRCT) developed in [1], based on [11,13] is a higher order continuum theory in which the expression for the principle of virtual internal power is extended. It is a general approach that includes many other formulations as subcases and can have multiple subscales.

MRCT provides a mathematical link between the materials macroscopic property and its microstructures across several distinct length scales. The evolution of the materials' microstructure can be evaluated at hierarchal subscales and coupled with the macroscopic deformation to predict the material behaviors and\or structural performances. It is then assumed that the inhomogeneous deformations occur at distinct subscales are directly included in the material constitutive equations of each subscale. This in turn also solves the notorious mesh dependent problem. The theory addresses the multi-scale nature of the material/structural responses required to predict the material behaviors [16].

3. Multiresolution continuum theory

The basic idea of a higher order continuum theory is that a point in the continuum is considered to be a deformable particle and a continuum is a collection of such deformable point particles. These point particles are infinitesimal in size but are assumed to have an inner structure which can be modeled as a sequence of nested microdomains for the material point $\mathbf{x}$. The formulation for MRCT is developed in terms of the virtual power in such a continuum during the deformation [17]

The linear approximation of the variation of the velocity field around a material point $\mathbf{x}$ in each microdomain shown in Fig. 1 is written as the first-order Taylor's series expansion about the center $\mathbf{x}$ of the microdomain to give

$$ {}_m\mathbf{l}^i(\mathbf{x}+\mathbf{y}) = \mathbf{l}^i(\mathbf{x}) + \mathbf{g}^i(\mathbf{x}) \times \mathbf{y}^i \tag{1} $$

where ${}_m\mathbf{l}^i$ denotes the local velocity gradient in each microdomain i. $\mathbf{y}^i$ is the local coordinate in the ith microdomain relative to the domain center. The term $\mathbf{l}^i$ is the volume average of the local velocity gradient and $\mathbf{g}^i$ is the gradient of micro-velocity gradient

$$ \mathbf{l}^i(\mathbf{x}) = \frac{1}{\boldsymbol{\Omega}^i} \int_{\Omega^i} {}_m\mathbf{l}^i \, d\boldsymbol{\Omega} \tag{2} $$

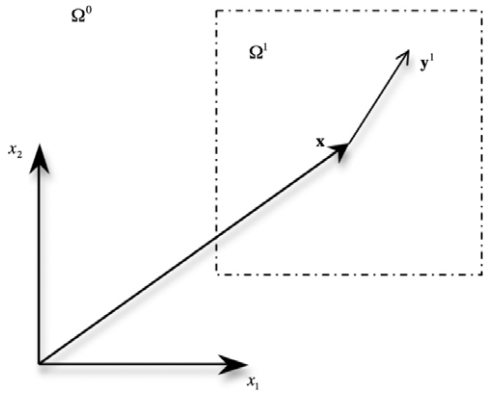

Fig. 1. A material point x with one microdomain Ω^1. Ω^0 is the macroscale.

$$\mathbf{g}^i(\mathbf{x}) = \frac{1}{\boldsymbol{\Omega}^i}\int_{\Omega^i}\frac{\partial_m \mathbf{l}^i}{\partial \mathbf{x}}d\boldsymbol{\Omega} \tag{3}$$

where Ω^i refers to the average volume at each scale.

The principle of virtual power [18] states that

$$\delta p_{\text{int}} = \delta p_{\text{ext}} \tag{4}$$

which holds at equilibrium for all admissible virtual velocities. For simplicity, we leave out the external virtual power as well as inertial effects in the following derivation of the MRCT element.

The deformation at the macroscale is coupled with the deformation at each subscale within the multiresolution continuum. The virtual internal power is now decomposed into two parts to account for both homogeneous and inhomogeneous deformations.

$$\delta p_{\text{int}} = \delta p_{\text{int}}^{\text{hom}} + \sum_{i=1}^{N}\delta p_{\text{int}}^{\text{inh}} \tag{5}$$

where N is the total number of subscales. The first term is the traditional homogenized virtual internal power. The second term arises from the inhomogeneous deformation in each microdomain and is defined as the difference between the volume average of local inhomogeneous virtual internal power and the virtual internal power at the macroscale, thus, we have

$$\delta p_{\text{int}}^{\text{hom}} + \delta p_{\text{int}}^{\text{inh}} = \boldsymbol{\sigma}^0 : \delta \mathbf{l}^0 + \sum_{i=1}^{N}\frac{1}{\Omega^i}\int_{\Omega^i}\left({}_m\boldsymbol{\sigma}^i : \delta_m \mathbf{l}^i - \boldsymbol{\sigma}^0 : \delta \mathbf{l}^0\right)d\Omega \tag{6}$$

where $\mathbf{l}^0$ is the spatial velocity gradient and $\boldsymbol{\sigma}^0$ is the Cauchy stress tensor at the macroscale. ${}_m\boldsymbol{\sigma}^i$ is the local stress in each microdomain i.

The inhomogeneous virtual internal power $\delta p_{\text{int}}^{\text{inh}}$ is approximated by

$$\begin{aligned}\delta p_{\text{int}}^{\text{inh}} &= \sum_{i=1}^{N}\frac{1}{\Omega^i}\int_{\Omega^i}\left({}_m\boldsymbol{\sigma}^i : \delta_m \mathbf{l}^i - \boldsymbol{\sigma}^0 : \delta \mathbf{l}^0\right)d\Omega \\ &= \sum_{i=1}^{N}\frac{1}{\Omega^i}\int_{\Omega^i}\left({}_m\boldsymbol{\beta}^i : \left(\delta_m \mathbf{l}^i - \delta \mathbf{l}^0\right)\right)d\Omega.\end{aligned} \tag{7}$$

The introduced local microstress ${}_m\boldsymbol{\beta}^i$ in the ith domain is the power conjugate to the local inhomogeneous velocity gradient $\left({}_m\mathbf{l}^i - \mathbf{l}^0\right)$. The relative virtual internal power ${}_m\boldsymbol{\sigma}^i : \delta_m \mathbf{l}^i - \boldsymbol{\sigma}^0 : \delta \mathbf{l}^0$ is studied in detail in the DNS region. The local stress ${}_m\boldsymbol{\sigma}^i$ and local velocity gradient ${}_m\mathbf{l}^i$ are calculated in each of the microdomains. The clear relationship

between the quantity $\left\| {}_m\boldsymbol{\sigma}^i : \delta_m\mathbf{l}^i - \boldsymbol{\sigma}^0 : \delta\mathbf{l}^0 \right\|$ and $\left\| {}_m\mathbf{l}^i - \mathbf{l}^0 \right\|$ has been shown and this motivates the introduction of the microstress ${}_m\boldsymbol{\beta}^i$. For detailed description please refer to [17].

The velocity gradient ${}_m\mathbf{l}^i$ in Eq. (1) in the microdomain is assumed to vary linearly with y^i. Therefore Eq. (7) can be written as

$$\begin{aligned}
\delta p_{int}^{\text{inh}} &= \sum_{i=1}^{N} \frac{1}{\Omega^i} \int_{\Omega^i} \left({}_m\boldsymbol{\beta}^i : \left(\delta_m\mathbf{l}^i - \delta\mathbf{l}^0 \right) \right) d\Omega \\
&= \sum_{i=1}^{N} \frac{1}{\Omega^i} \int_{\Omega^i} \left({}_m\boldsymbol{\beta}^i : \left(\delta\mathbf{l}^i + \delta\mathbf{g}^i \cdot \mathbf{y}^i - \delta\mathbf{l}^0 \right) \right) d\Omega \\
&= \sum_{i=1}^{N} \frac{1}{\Omega^i} \int_{\Omega^i} \left({}_m\boldsymbol{\beta}^i : \left(\delta\mathbf{l}^i - \delta\mathbf{l}^0 \right) \right) d\Omega + \frac{1}{\Omega^i} \int_{\Omega^i} \left(\left({}_m\boldsymbol{\beta}^i \otimes \mathbf{y}^i \right) \vdots \delta\mathbf{g}^i \right) d\Omega \\
&= \sum_{i=1}^{N} \boldsymbol{\beta}^i : \left(\delta\mathbf{l}^i - \delta\mathbf{l}^0 \right) + \mathbf{m}^i \vdots \delta\mathbf{g}^i .
\end{aligned} \tag{8}$$

Two new terms have been introduced above: (1) the microstress $\boldsymbol{\beta}^i$ and (2) the microstress couple $\mathbf{m}^i$. These microstress quantities are related to the local microstress ${}_m\boldsymbol{\beta}^i$ by

$$\begin{aligned}
\boldsymbol{\beta}^i &= \frac{1}{\Omega^i} \int_{\Omega^i} {}_m\boldsymbol{\beta}^i d\Omega \\
\mathbf{m}^i &= \frac{1}{\Omega^i} \int_{\Omega^i} {}_m\boldsymbol{\beta}^i \otimes \mathbf{y} d\Omega .
\end{aligned} \tag{9}$$

Now, the total virtual internal power integrated over the entire body is written as:

$$\delta p_{int} = \delta p_{int}^{\text{hom}} + \delta p_{int}^{\text{inh}} = \int_{\Omega} \left(\boldsymbol{\sigma}^0 : \delta\mathbf{l}^0 + \sum_{i=1}^{N} \left(\boldsymbol{\beta}^i : \delta\left(\mathbf{l}^i - \mathbf{l}^0 \right) + \mathbf{m}^i \vdots \delta\mathbf{g}^i \right) \right) d\Omega . \tag{10}$$

The virtual velocity gradient can be split into a symmetric part $\mathbf{d}$ and a skew symmetric part $\mathbf{w}$. $\mathbf{d}$ is the rate of deformation tensor and $\mathbf{w}$ is the spin tensor. During the deformation the rotation of the microdomain with respect to the macroscopic domain is ignored [16]. Then the expression for the virtual power becomes

$$\delta p_{int} = \delta p_{int}^{\text{hom}} + \delta p_{int}^{\text{inh}} = \int_{\Omega} \left(\boldsymbol{\sigma}^0 : \delta\mathbf{d}^0 + \sum_{i=1}^{N} \left(\boldsymbol{\beta}^i : \delta\left(\mathbf{d}^i - \mathbf{d}^0 \right) + \mathbf{m}^i \vdots \delta\mathbf{g}_d^i \right) \right) d\Omega \tag{11}$$

where $\delta\mathbf{g}_d^i$ represents the symmetric part of $\mathbf{g}^i$. As the product of the symmetric stress tensor $\boldsymbol{\sigma}^0$ and skew symmetric spin tensor $\mathbf{w}$ is zero. Inserting Eq. (11) into Eq. (4) and using integration by parts and Gauss's theorem leads to

$$\begin{aligned}
\delta p_{\text{int}} = &- \int_{\Omega} \left\{ \nabla \left(\boldsymbol{\sigma}^0 - \sum_{i=1}^{N} \boldsymbol{\beta}^i \right) \cdot \delta\mathbf{v}^0 + \sum_{i=1}^{N} \left(\nabla\mathbf{m}^i - \boldsymbol{\beta}^i \right) : \delta\mathbf{d}^i \right\} d\Omega \\
&+ \int_{S} \left(\boldsymbol{\sigma}^0 - \sum_{i=1}^{N} \boldsymbol{\beta}^i \right) \cdot \mathbf{n} \cdot \delta\mathbf{v}^0 dS + \int_{S} \sum_{i=1}^{N} \left(\mathbf{m}^i \cdot \mathbf{n} \right) : \delta\mathbf{d}^i dS = 0.
\end{aligned} \tag{12}$$

$\boldsymbol{\delta}\mathbf{v}^0$ is the macroscale virtual velocity, which arises from integrating by parts the power conjugate pairs at each scale. $\mathbf{n}$ and S arise from the application of Gauss's theorem, S is the surface enclosing the volume and $\mathbf{n}$ is the outward pointing unit normal. Eq. (12) should be valid for all admissible velocity fields. Thus, we obtain

$$\begin{aligned}
&\nabla \cdot \left(\boldsymbol{\sigma}^0 - \sum_{i=1}^{N} \boldsymbol{\beta}^i \right) = 0 \\
&\nabla \cdot \mathbf{m}^i - \boldsymbol{\beta}^i = 0,
\end{aligned} \tag{13}$$

with boundary conditions:

$$\left(\boldsymbol{\sigma}^0 - \sum_{i=1}^{N} \boldsymbol{\beta}^i\right) \cdot \mathbf{n} = 0$$
$$\mathbf{m}^i \cdot \mathbf{n} = 0. \tag{14}$$

MRCT is a general framework that can degenerate into many other deformation theories in certain circumstances. The above relations, after including possible external loadings, are a generalization of the classical continuum mechanics theory. The conventional continuum theory is recovered upon setting $N = 0$. Furthermore, a micromorphic model [13] can be retrieved when the material in question only possesses two length scales. If the anti-symmetric part of the local inhomogeneous velocity gradient $\left(\mathbf{l}^i - \mathbf{l}^0\right)$ and the gradient of micro-velocity gradient $\mathbf{g}^i$ is taken as the power conjugate of microstress $\boldsymbol{\beta}^i$ and microstress couple $\mathbf{m}^i$, respectively, then the Cosserat theory [11] is retrieved. The general equilibrium relations above are complemented by the constitutive relations described next.

4. Constitutive models

The material in the current paper is assumed to have two scales, one macroscopic scale and one subscale. A hypoelastic–plastic approach is used in the stress update algorithm and the formulation accommodates large strains. The macroscopic properties are described either by an elastic–plastic hardening law or a linear strain softening law. The subscale can accommodate hardening and this makes it also possible to obtain the convergent solutions for localization problems, which is demonstrated below. A very simple elastic-damage model is used in the microdomain but it can easily be replaced by more appropriate models for simulating real cases. We focus on the numerical aspects in the current paper. Therefore, we do not discuss the actual models and values used in depth in this paper.

4.1. Multiresolution constitutive relations

All stress and strain measures in multiresolution continuum are included in the generalized multiresolution stress vector

$$\boldsymbol{\Sigma}^T = \left[\boldsymbol{\sigma}^0 \quad \boldsymbol{\beta}^i \quad \mathbf{m}^i\right] \tag{15}$$

and a generalized multiresolution strain vector

$$\boldsymbol{\Delta}^T = \left[\mathbf{d}^0 \quad \mathbf{d}^i - \mathbf{d}^0 \quad \mathbf{g}_d^i\right]. \tag{16}$$

The multiresolution continuum elastic matrix $\mathbf{C}$ relates the objective rates of the generalized stress vector and the elastic part of the generalized strain vector

$$\boldsymbol{\Sigma}^{\nabla} = \mathbf{C} \cdot \boldsymbol{\Delta}^e. \tag{17}$$

$\mathbf{C}$ is written as

$$C = \begin{bmatrix} \mathbf{C}_\sigma & 0 & 0 \\ 0 & \mathbf{C}_\beta^i & 0 \\ 0 & 0 & \mathbf{C}_{\mathrm{m}}^i \end{bmatrix}. \tag{18}$$

$\mathbf{C}_\sigma$ is the conventional elasticity tensor (Hooke's law), $\mathbf{C}_\beta^i$ and $\mathbf{C}_{\mathrm{m}}^i$ are the elastic moduli in each microdomain given by

$$\mathbf{C}_{\boldsymbol{\beta}}^i = \frac{1}{\Omega^i} \int_{\Omega^i} {}_m\mathbf{C}^a d\Omega = \mathbf{C}^a$$
$$\mathbf{C}_{\mathrm{m}}^i = \frac{1}{\Omega^i} \int_{\Omega^i} {}_m\mathbf{C}^a \otimes \mathbf{y} \otimes \mathbf{y} d\Omega = \mathbf{C}^a \otimes \frac{l^{i2}}{12}\mathbf{I}. \tag{19}$$

I is the identity matrix, $\mathbf{C}^a$ is the volume average of local elasticity tensor in the microdomain. Choosing the elastic properties is still somewhat of an ad-hoc procedure [2] and in current paper $\mathbf{C}^a = \frac{1}{10}\mathbf{C}_\sigma$ is employed. One of the key features of the MRCT is that the length scale parameter l^i for each microdomain, which is the length of one side of the averaging volume Ω^i, has been directly incorporated into the multiresolution continuum constitutive relations Eq. (19) which is absent in conventional continuum mechanics method.

4.2. Macroscopic plastic behavior

There are different ways of treating MRCT plastic behaviors. One way is to use a single plastic potential, which is a function of the generalized stress vector and the generalized internal state variables vector [19,20]. Another way is to use a multiple plastic potentials method in which the plastic potential at each scale is treated separately [1,20]. In our current implementation, we use the multiple plastic potentials method.

A classical finite deformation J_2 flow theory with a general saturation isotropic hardening law is used to model the flow stress at the macroscopic scale in the problem demonstrated in Section 6.1.

$$\sigma_y = \sigma_\infty + (\sigma_0 - \sigma_\infty)\exp\left(-\beta\bar{\varepsilon}^{pl}\right) + H_{iso}\bar{\varepsilon}^{pl}, \tag{20}$$

where σ_y is the flow stress, σ_0 is the initial uniaxial yield stress, σ_∞ is a stress at large values of strain, β is called the delay constant, H_{iso} is the linear isotropic hardening modulus and $\bar{\varepsilon}^{pl}$ is the equivalent plastic strain.

The plastic flow rule and evolution equations are given in [21] as

$$\begin{aligned} \dot{\mathbf{d}}^p &= \dot{\lambda}\mathbf{r} \\ \mathbf{r} &= \frac{3}{2\bar{\sigma}}\boldsymbol{\sigma}^{dev} \\ \dot{\lambda} &= \dot{\bar{\varepsilon}}^{pl}, \end{aligned} \tag{21}$$

where $\dot{\mathbf{d}}^p$ is the plastic part of macroscopic rate of deformation, the plastic parameter $\dot{\lambda}$ is equal to the rate of effective plastic strain, $\mathbf{r}$ is the flow direction, $\boldsymbol{\sigma}^{\mathrm{dev}}$ is the deviatoric stress and $\bar{\sigma}$ is the von Mises effective stress. The radial return method is used to update the stresses and internal state variables. In order to obtain the quadratic convergence rate when using Newton–Raphson iterations for solving the global equilibrium equations, the algorithmic modulus is needed. It is calculated as

$$\mathbf{C}_\sigma^{al} = \left(\frac{\partial\boldsymbol{\sigma}}{\partial\boldsymbol{\varepsilon}}\right)_{n+1}. \tag{22}$$

4.3. Elastic-damage in the microdomain

The microdomain is assumed to be either elastic with damage in the problem demonstrated in Section 6.1 or pure elastic in the problem in Section 6.4. Fig. 2 is a two dimensional view of damage in the microdomain. The parameter y_i^d is the distance from the origin to the location at which the damage has extended to within the microdomain. For simplicity, y_i^d is assumed to be symmetric. Thus $y_i^d = y_i^- = y_i^+$.

The damaged region is assumed to have completely lost its load carrying capacity and consequently the homogenized elastic matrices with damage for the microdomain are rewritten as

$$\begin{aligned} \mathbf{C}_\beta^1 &= \mathbf{C}^a\prod_{i=1}^{3}(1-\omega_i) = \mathbf{C}^a Z_1 Z_2 Z_3 \\ \mathbf{C}_{\mathrm{m}}^1 &= \mathbf{C}^a \otimes \frac{\left(l^1\right)^2}{12}\mathbf{D}, \end{aligned} \tag{23}$$

where

$$Z_i = \frac{2y_i}{l^1} = 1 - \omega_i \tag{24}$$

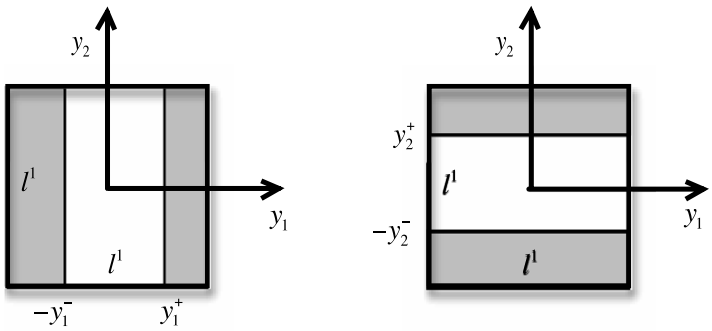

Fig. 2. Two-dimensional view of damage volumes (gray) that are growing into the microdomain.

and

$$\mathbf{D} = \begin{bmatrix} (Z_1)^3 Z_2 Z_3 & 0 & 0 \\ 0 & Z_1 (Z_2)^3 Z_3 & 0 \\ 0 & 0 & Z_1 Z_2 (Z_3)^3 \end{bmatrix}, \tag{25}$$

where ω_i is the fraction of the length that is damaged. The equivalent plastic strain at the macroscale is assumed to govern the damage in the subscale.

$$\omega = \omega_1 = \omega_2 = \omega_3 = \left\langle \frac{\bar{\varepsilon}^{pl} - \varepsilon_{init}}{\varepsilon_{fracture} - \varepsilon_{init}} \right\rangle. \tag{26}$$

Thus, we assume that the damage grows equally in all 3 directions. The symbol $\langle\rangle$ denotes that the expression is zero for negative arguments. ε_{init} and $\varepsilon_{fracture}$ are the effective damage initiation strain and the fracture strain, respectively. More advanced damage models which may include stress or strain components such that damage can vary in different directions within the microdomain can be used.

5. The implicit MRCT 3D element with one subscale

5.1. Finite element formulation

The nodal velocities give the macroscopic strain rate $\mathbf{d}^0$ in Eq. (16). Spin is ignored in the microdomain as stated in the previous section so only the symmetric part of microscopic velocity gradient is used.

There are 9 degrees of freedom per node for the 3D MRCT element, 3 macroscopic velocities $\mathbf{v}^0$ and 6 velocity gradients $\mathbf{d}_i^1$ at the subscale. The element interpolation of the nodal values is

$$\mathbf{v}_e = \sum_{i=1}^{nnode} \begin{bmatrix} \mathbf{N}^0 & 0 \\ 0 & \mathbf{N}^1 \end{bmatrix}_i \begin{bmatrix} \mathbf{v}^0 \\ \mathbf{d}^1 \end{bmatrix}_i = \mathbf{N}\mathbf{v}. \tag{27}$$

$\mathbf{N}^0$ and $\mathbf{N}^1$ indicate that we may use different functions to interpolate the nodal velocities than the microscopic quantities. Likewise, we may use a different number of integration points during numerical integration. The current implementation is based on $\mathbf{N}^1 = \mathbf{N}^0$. The necessary rates of the macroscopic velocity gradient, microscopic velocity gradient and the gradient of the microscopic velocity gradient can be written as:

$$\begin{aligned} \mathbf{d}^0(\mathbf{x}) &= \mathbf{B}^0\mathbf{v}^0 \\ \mathbf{d}^1(\mathbf{x}) &= \mathbf{N}^1\mathbf{d}^1 \\ \mathbf{g}_d^1(\mathbf{x}) &= \mathbf{G}^1\mathbf{d}^1. \end{aligned} \tag{28}$$

Thus the gradient of the micro-velocity gradient tensor $\mathbf{g}_d^1$ is not an independent variable but is calculated as the gradient of $\mathbf{d}^1(\mathbf{x})$ within the element. $\mathbf{B}^0$ and $\mathbf{G}^1$ are the macroscopic and microscopic spatial derivatives of the mapping functions.

The generalized strain rate vector is written as

$$\Delta = \begin{bmatrix} \mathbf{d}^0 \\ \mathbf{d}^1 - \mathbf{d}^0 \\ \mathbf{g}^1 \end{bmatrix} = \begin{bmatrix} \mathbf{B}^0 & 0 \\ -\mathbf{B}^0 & \mathbf{N}^1 \\ 0 & \mathbf{G}^1 \end{bmatrix} \begin{bmatrix} \mathbf{v}^0 \\ \mathbf{d}^1 \end{bmatrix} = \mathbf{Q}\mathbf{v}. \tag{29}$$

The continuum internal forces are calculated as:

$$\mathbf{f}_{\text{int}} = \int_\Omega \mathbf{Q}^T \Sigma d\Omega = \int_\Omega \begin{bmatrix} \left(\mathbf{B}^0\right)^T \left(\boldsymbol{\sigma}^0 - \boldsymbol{\beta}^1\right) \\ \left(\mathbf{N}^1\right)^T \boldsymbol{\beta}^1 + \left(\mathbf{G}^1\right)^T \mathbf{m}^1 \end{bmatrix} d\Omega. \tag{30}$$

The material tangent stiffness matrix for MRCT element is written as:

$$\begin{aligned} \mathbf{K}_{mat} &= \int_\Omega \mathbf{Q}^T \mathbf{C}^{al} \mathbf{Q} d\Omega \\ &= \int_\Omega \begin{bmatrix} \left(\mathbf{B}^0\right)^T & -\left(\mathbf{B}^0\right)^T & 0 \\ 0 & \left(\mathbf{N}^1\right)^T & \left(\mathbf{G}^1\right)^T \end{bmatrix} \begin{bmatrix} \mathbf{C}_\sigma^{al} & 0 & 0 \\ 0 & \mathbf{C}_\beta^{al1} & 0 \\ 0 & 0 & \mathbf{C}_{\text{m}}^{al1} \end{bmatrix} \begin{bmatrix} \mathbf{B}^0 & 0 \\ -\mathbf{B}^0 & \mathbf{N}^1 \\ 0 & \mathbf{G}^1 \end{bmatrix} d\Omega \\ &= \int_\Omega \begin{bmatrix} \left(\mathbf{B}^0\right)^T \mathbf{C}_\sigma^{al} \mathbf{B}^0 + \left(\mathbf{B}^0\right)^T \mathbf{C}_\beta^{al1} \mathbf{B}^0 & -\left(\mathbf{B}^0\right)^T \mathbf{C}_\beta^{al1} \mathbf{N}^1 \\ -\left(\mathbf{N}^1\right)^T \mathbf{C}_\beta^{al1} \mathbf{B}^0 & \left(\mathbf{N}^1\right)^T \mathbf{C}_\beta^{al1} \mathbf{N}^1 + \left(\mathbf{G}^1\right)^T \mathbf{C}_{\text{m}}^{al1} \mathbf{G}^1 \end{bmatrix} d\Omega, \end{aligned} \tag{31}$$

where $\mathbf{C}_\sigma^{al}$, $\mathbf{C}_\beta^{al1}$ and $\mathbf{C}_{\text{m}}^{al1}$ are algorithmic moduli for the macroscopic and microscopic scales and are calculated separately at each scale.

The geometric part of the consistent tangent has only been added to the macroscopic part of the element. This may improve convergence in presence of large rotation of a stressed body. The MRCT tangent stiffness matrix becomes then

$$\mathbf{K} = \int_\Omega \begin{bmatrix} \mathbf{K}^0 + \left(\mathbf{B}^0\right)^T \mathbf{C}_\beta^{al1} \mathbf{B}^0 & -\left(\mathbf{B}^0\right)^T \mathbf{C}_\beta^{al1} \mathbf{N}^1 \\ -\left(\mathbf{N}^1\right)^T \mathbf{C}_\beta^{al1} \mathbf{B}^0 & \left(\mathbf{N}^1\right)^T \mathbf{C}_\beta^{al1} \mathbf{N}^1 + \left(\mathbf{G}^1\right)^T \mathbf{C}_{\text{m}}^{al1} \mathbf{G}^1 \end{bmatrix} d\Omega, \tag{32}$$

where

$$\mathbf{K}^0 = \mathbf{B}^{0T} (\mathbf{C}_{\boldsymbol{\sigma}}^{al} - \tilde{\boldsymbol{\sigma}}) \mathbf{B}^0 + \mathbf{G}^{0T} \hat{\boldsymbol{\sigma}} \mathbf{G}^0. \tag{33}$$

The detailed expressions of $\tilde{\boldsymbol{\sigma}}$, $\hat{\boldsymbol{\sigma}}$ and $\mathbf{G}^0$ are listed in [22].

5.2. Implementation in FEAP

The above theory for a MRCT element has been implemented in the general purpose finite element analysis program FEAP [7]. We use the hypoelastic–plastic approach for stress updating as described above. The stress updating routine for the macroscopic scale and the subscale are put into two separate user-defined material subroutines, *umatl3.f* and *umatl4.f*, driven by the MRCT element subroutine defined as the user element *elmt42.f* in FEAP. The flow chart for the relevant user subroutines implemented in FEAP is given in the Appendix.

6. Demonstration of MRCT element

The following example, often used in the literature, is used to verify the coding of the implicit MRCT element. A 3-D bar is subjected to a tensile load by prescribing the displacement of its ends. Due to symmetry, only one eighth of the geometry is modeled and the mesh is shown in Fig. 3.

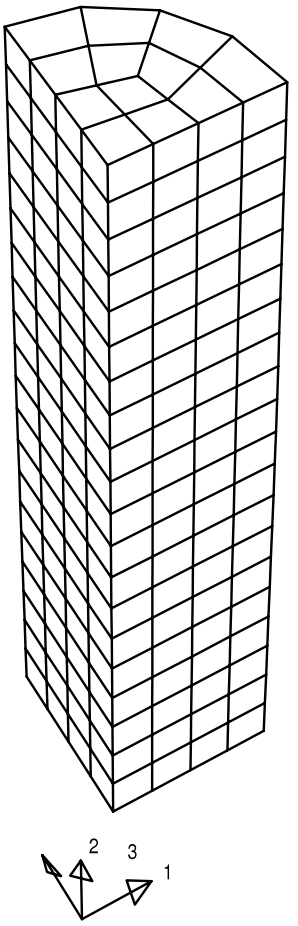

Fig. 3. Mesh of a 3D bar under tension.

The geometry and the material properties of the bar are consistent with that used in Simo [23]. The total length of the bar is $L = 53.334$ mm and the radius of the bar is $R = 6.413$ mm. The radius of the cross-section in the middle of the bar is reduced by a factor of $f = 0.982$ to trigger the localization. The Young's modulus is taken as $E = 206.9$ GPa and the Poisson's ratio is $\nu = 0.29$. The material constants in Eq. (20) are taken as follows:

$$\sigma_0 = 0.45 \text{ GPa} \qquad \sigma_\infty = 0.715 \text{ GPa} \qquad \beta = 16.93 \qquad H_{iso} = 0.12924 \text{ GPa}.$$

The final axial elongation in the pulling direction (direction 3 in Fig. 3) is 6 mm except for the case when comparing to the explicit MRCT element where it is 5.4 mm. The higher order boundary conditions are set to zero, which are unconstrained degrees of freedom. Physically this means the inhomogeneous deformation disappears on the boundary.

6.1. Tensile test result

Fig. 4 shows the variation in tensile stress with different length scales along the center axis of the bar. *feap20* denotes the solution obtained when using the large deformation subroutine which is automatically provided by FEAP. *ubar20* denotes the result obtained by using our implementation of the hypoelastic–plastic subroutine with only the macroscopic part of the MRCT element. These results are given to verify the coding of the macroscopic part of the MRCT element subroutine. *m20L2*, m*20L4* and *m20L6* represent the results obtained using MRCT elements with the length scale in Eq. (19) set to 2, 4 and 6, respectively. *m20* simply indicates that the bar is discretized into 20 layers in the pulling direction which is a description of how well the mesh is refined, see Fig. 3. The length scales used (2, 4 and 6) are all larger than the smallest element size. As we can see in the figure, smaller length scales yield smaller values of damage and thus have less of an effect on the stress distribution. This also means that when a real

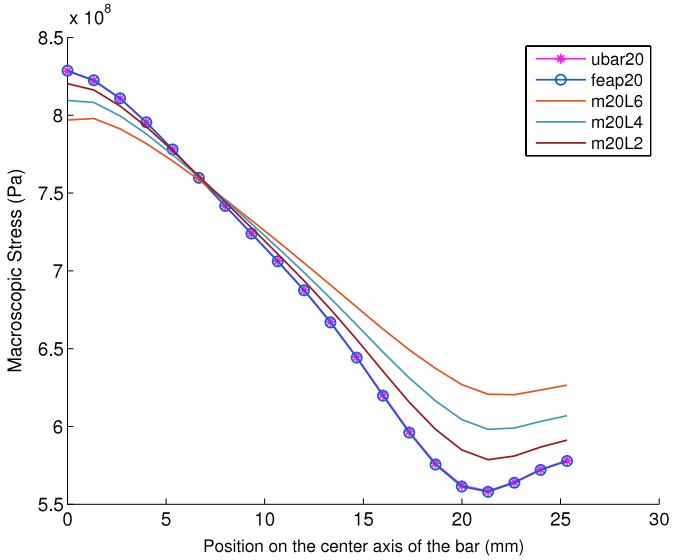

Fig. 4. Tensile stress at different length scales along the center axis of the bar.

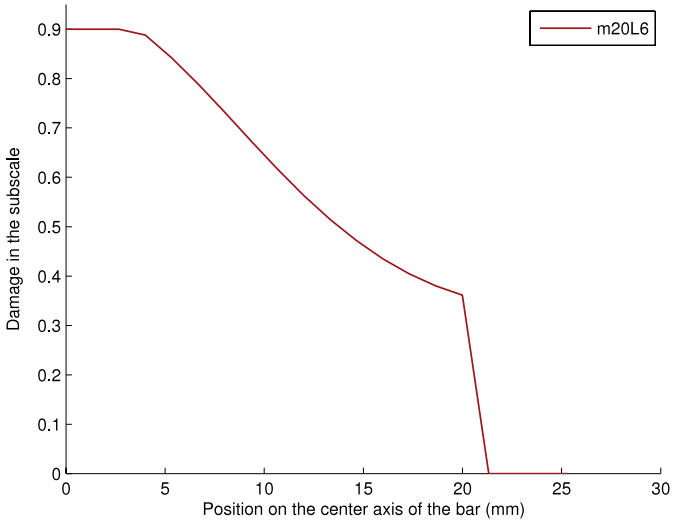

Fig. 5. Damage in the subscale along the center axis of the bar.

case is modeled the damage parameters must be selected based on the given length scale. A change in the length scale will affect the damage distribution.

Damage along the center axis of the bar in the material subscale is plotted in Fig. 5. The damage is highest in the center region and is zero further away from the localization. This causes the macroscopic stresses to be reduced in this region compared to the *feap20* and *ubar20* in Fig. 4. Without damage, the subscale is elastic, which explains why the macroscopic stress furthest away from the center region becomes higher than that at positions just less than the end of the bar (e.g., compare positions 21 mm and 25 mm from the center of the bar).

6.2. Convergence rate of MRCT element

The use of the multiresolution consistent tangent in Eq. (32) should ensure 2nd order convergence in the global equilibrium iterations when using a full Newton–Raphson solver. The force displacement plot for the MRCT element used for the problem described in the beginning of chapter 6 with 240 elements and a length scale of 2 is shown in

Table 1
Convergence rate of the MRCT element.

Step	Number of iterations	Residual norm
11	1	3.4352689E−02
11	2	8.0821923E−02
11	3	2.0131921E−03
11	4	5.9713758E−05
11	5	8.3360297E−08
11	6	1.4531915E−10
576	1	4.4649145E−02
576	2	9.7728188E−06
576	3	2.5410848E−08
576	4	2.4476000E−10
1000	1	4.8782310E−02
1000	2	5.8001274E−02
1000	3	1.4411513E−03
1000	4	8.8169940E−04
1000	5	4.8016347E−04
1000	6	2.1728367E−04
1000	7	8.6925456E−05
1000	8	2.4316621E−05
1000	9	3.4661472E−06
1000	10	8.5144380E−09

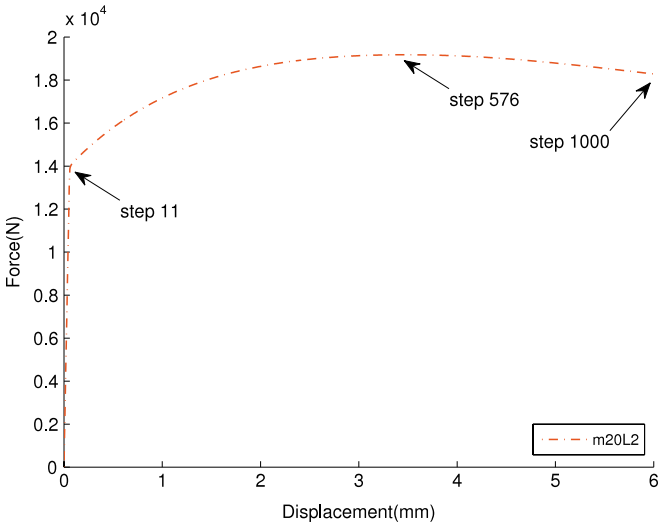

Fig. 6. Force displacement plot of MRCT element with a length scale of 2.

Fig. 6. The convergence rate in Table 1 is given for the three time instances marked in this figure. It can be shown via Table 1 that the convergence rate is in fact 2nd order until the end of the analysis.

6.3. Comparison with the explicit version of MRCT element

The above implicit implementation of the MRCT element is compared with the explicit version of the code in order to validate the microdomain implementation. This also serves as a comparison between the explicit and implicit formulations of for quasistatic cases. In this case, the bar is pulled to 5.4 mm instead of 6 mm due to the excessive dynamic responses of the explicit code. The macroscopic stresses, denoted expmul and impmul, are plotted in Fig. 7. They are obtained from the MRCT explicit and implicit codes, respectively, using the same length scale. The results

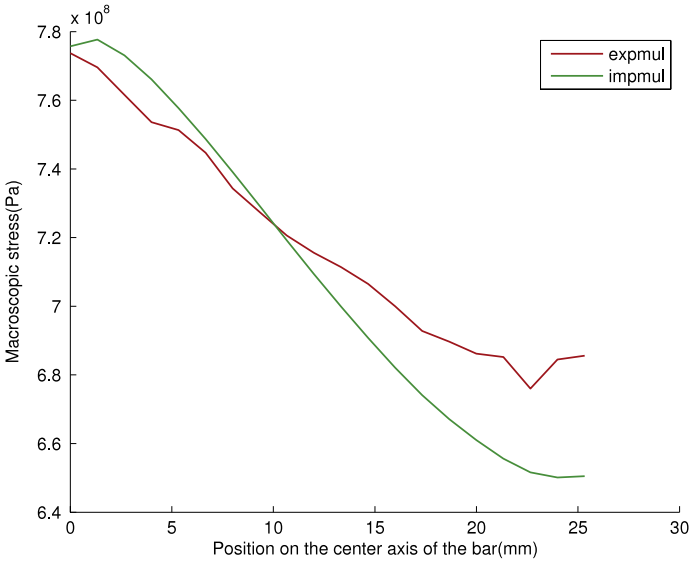

Fig. 7. Comparison of the macroscopic stress given by the explicit and implicit MRCT element.

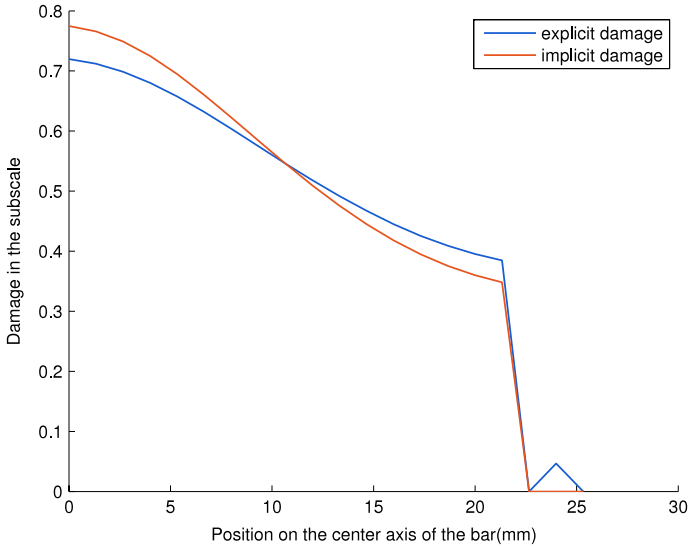

Fig. 8. Comparison of the subscale damage given by the explicit and implicit MRCT element.

bear some resemblance. However, there are some dynamic influences on the results for the explicit code. The subscale damage of the two codes is plotted in Fig. 8. The damage predicted by the two elements is also observed to be similar.

6.4. Mesh independent solutions and length scale

The problem described in beginning of chapter 6 is modified in order to introduce a stronger softening behavior. The problem is used to demonstrate the mesh independent results that can be obtained due to the length-scale in the MRCT element. Linear strain softening in the macroscopic constitutive behavior of the material is introduced. The example can be found in [5]. The subscale is purely elastic without damage. The macroscopic Young's modulus is $E = 80$ GPa, Poisson's ratio is $\nu = 0.29$, initial yield stress is $\sigma_0 = 0.160$ GPa and the linear softening modulus is

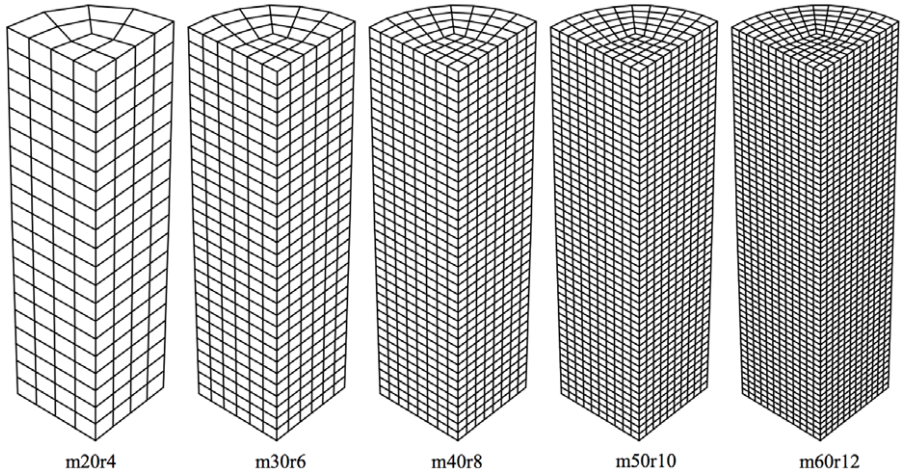

Fig. 9. Refined mesh with more elements.

−0.150 GPa [5]. The boundary conditions used here are the same as the previous problem except that the final axial elongation in the pulling direction is 1 mm.

The mesh is refined such that there are more elements to use in checking the length scale effect on the mesh sensitivity of the MRCT element. The refined meshes are shown in Fig. 9. The number following the letter *m* refers to the division of the mesh in z direction. The number after letter *r* refers to the division of the mesh in the radius of the bar. Length scale parameter is taken as $L = 10$, so that it is fully resolved in the each of the mesh discretizations.

The effective plastic strain along the center axis of the bar for different mesh discretizations is plotted in Fig. 10. *m20r4, m30r6*, *m40r8, m50r10, m60r12* represent the results predicted by conventional continuum method, while *m20r4L10*, *m30r6L10, m40r8L10, m50r10L10* and *m60r12L10* are predicted by the MRCT element with length scale 10. It shows clearly that the results predicted by the conventional continuum methods are dependent upon the mesh as opposed the results predicted by the MRCT element, which gives the mesh independent solution. We have in the current case used a rather large length scale in the MRCT element as it is necessary to resolve this length scale in order to obtain a mesh independent solution.

Fig. 11 shows how changing the length scale affects the deformation. *m40* represents the result predicted by the conventional finite element, the rest of the curves are the results predicted by the MRCT element with different length scales for the same mesh. *L001*, *Lele*, *L1*, *L3* and *L10* here simply mean the length scale parameter is taken as 0.01, element size, 1, 3 and 10 respectively. The length scale parameter determines the localization behavior.

The results in terms of force–displacement are shown in Fig. 12. Mesh sensitivity is expected for curves *m20r4, m30r6*, *m40r8, m50r10* and *m60r12,* which are predicted by conventional continuum method. The more the mesh is refined the steeper the slope of the curve is. The curves predicted by MRCT element remain close and have the same slope. Fig. 13 is the magnified force displacement plot of Fig. 12. We can see that the slopes are the same for MRCT elements as opposed to the results predicted by conventional continuum method. The MRCT results are converging.

7. Conclusions and discussion

- The implementation of an implicit MRCT element into FEAP has been verified. It is a general formulation for higher order continuum theory and can accommodate several other types of formulations. It can accommodate multiple scales, as shown in the works by Liu and coworkers.
- The merit of the implicit MRCT element compared to the explicit version is that no dynamic vibrations show up when modeling quasistatic problems.
- The element shows second order convergence in the equilibrium iterations verifying the formulation of the element tangent matrix.

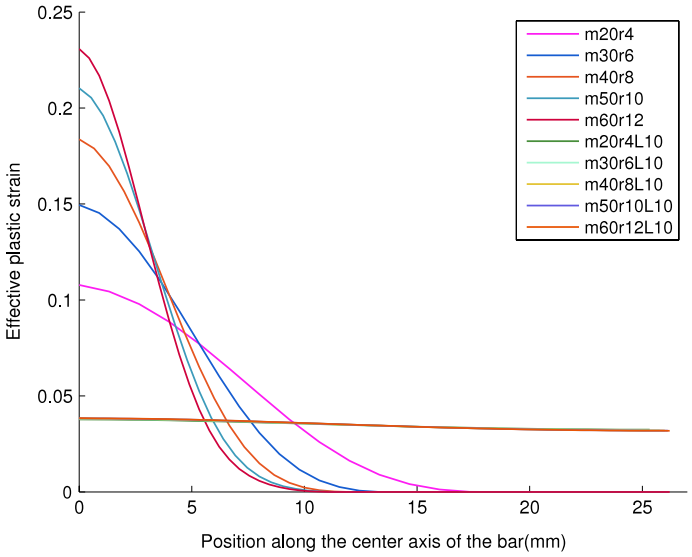

Fig. 10. Equivalent plastic strain along the center axis of the bar with length scale of 10 for different mesh discretizations.

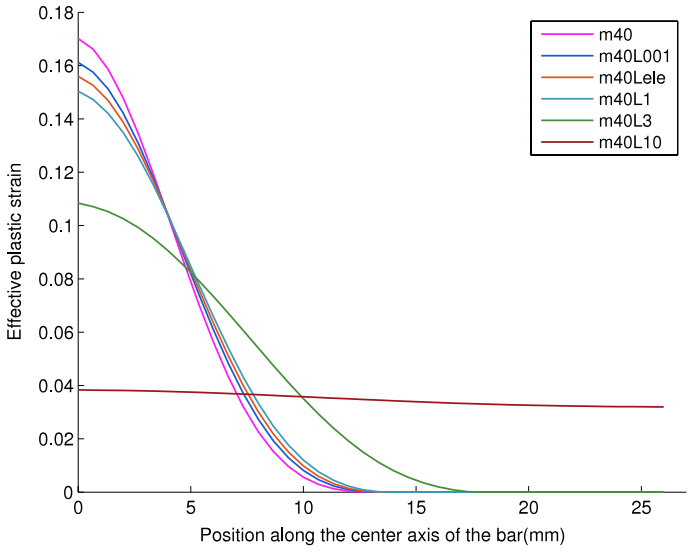

Fig. 11. Results predicted by different length scale parameter for the same mesh.

- The element can be used to obtain mesh independent results in the case of deformation localization when choosing an appropriate length scale associated with the microdomain. The mesh needs to be refined to fully resolve the length scale.
- The length scale of the microdomain should be related to the physics of the problem at hand. However, it can also be used as a numerical regularization parameter to obtain mesh independent results.

It is not obvious how to calibrate the constitutive behavior of the microdomain. One can note from the evaluations above that the used properties must be related to the chosen length scale. In future work, the implicit MRCT element will be applied to the problem of fracturing of high strength steels where the constitutive behavior need to be addressed more in detail.

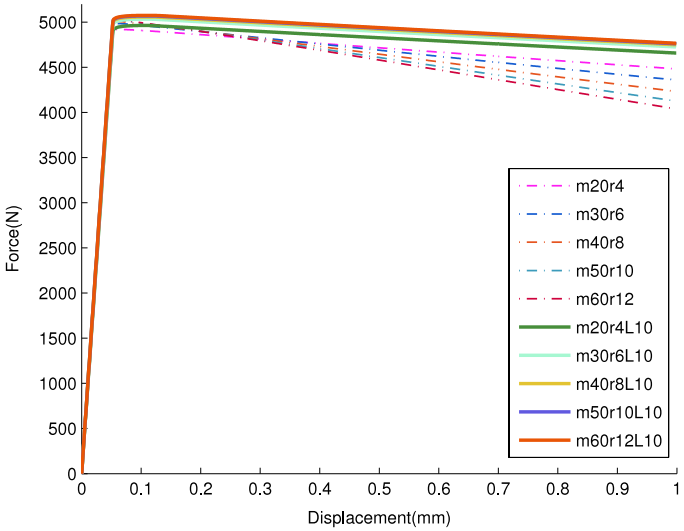

Fig. 12. Force displacement plot.

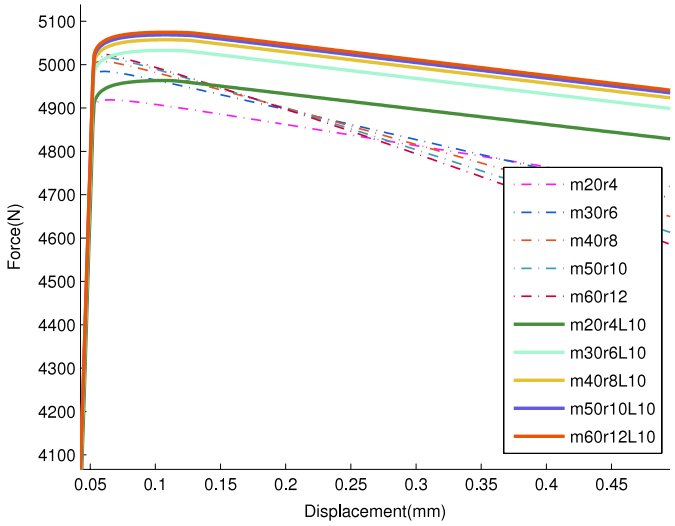

Fig. 13. Magnified force displacement plot.

Acknowledgments

The authors gratefully acknowledge the support of CHS (Center of High Performance Steels) of Luleå University of Technology and Swedish Steel Research Program. This work was also performed under the following financial assistance award 70NANB14H012 from U.S. Department of Commerce, National Institute of Standards and Technology as part of the Center for Hierarchical Materials Design (CHiMaD).

Appendix

The main steps of the implementation of the multiresolution element into FEAP are listed in Tables A.1 and A.2, respectively.

Table A.1
Main steps in MRCT user element subroutine *elmt42.f*.

Subroutine *elmt42*
Call 3D Gauss quadrature routine to retrieve element quadrature point information
Enter loop covering all integration points in the element
Call shape function routine to calculate the shape functions $\mathbf{N}_i$, the Cartesian shape function derivatives and the determinant of the Jacobian matrix
Call strain matrix routine to calculate mid-point strain increment at the macroscopic scale and at the subscale. Calculate the macroscopic spin increment
Call *umatl3*.f to update macroscopic stresses and calculate the macroscopic algorithmic modulus. Stress rotation is calculated according to *local rotated representation* [24] to ensure incremental objectivity
Call *umatl4*.f to update microscopic stresses and damage in the subscale. Incrementally objective microstresses are ensured with *local rotated representation* as well
Call a routine to evaluate the internal forces based on Eq. (30)
Call a routine to assemble the multiresolution tangent stiffness matrix based on Eq. (32)
End integration loop
End subroutine *elmt42*

Table A.2
Main steps of macroscopic stress updating subroutine *umatl3.f*.

Subroutine *umatl3*
Set the material parameters
Retrieve the history data from previous time step n.
Call a stress rotation routine to rotate $\boldsymbol{\sigma}_n$ and the macroscopic strain increment $\mathbf{d}^0$ based on [24].
Compute the deviatoric trial stress.
Check for yielding.
If yielding, then apply the radial return method to update the stresses to get $\boldsymbol{\sigma}_{n+1}$. Algorithmic modulus $\mathbf{C}_{\sigma}^{al}$ is evaluated here.
If not yielding, elastic step.
End subroutine *umatl3*

References

[1] F. Vernerey, W.K. Liu, B. Moran, Multi-scale micromorphic theory for hierarchical materials, J. Mech. Phys. Solids 55 (12) (2007) 2603–2651.
[2] F.J. Vernerey, W.K. Liu, B. Moran, G. Olson, A micromorphic model for the multiple scale failure of heterogeneous materials, J. Mech. Phys. Solids 56 (4) (2008) 1320–1347.
[3] C. McVeigh, W.K. Liu, Linking microstructure and properties through a predictive multiresolution continuum, Comput. Methods Appl. Mech. Eng. 197 (41–42) (2008) 3268–3290.
[4] R. Tian, S. Chan, S. Tang, A.M. Kopacz, J. Wang, H. Jou, L. Siad, L. Lindgren, G.B. Olson, W.K. Liu, A multiresolution continuum simulation of the ductile fracture process, J. Mech. Phys. Solids 58 (10) (2010) 1681–1700.
[5] C.J. McVeigh, Linking properties to microstructure through multiresolution mechanics, 2007.
[6] S. Tang, A.M. Kopacz, S. Chan O'Keeffe, G.B. Olson, W.K. Liu, Three-dimensional ductile fracture analysis with a hybrid multiresolution approach and microtomography, J. Mech. Phys. Solids 61 (11) (2013) 2108–2124.
[7] O.C. Zienkiewicz, R.L. Taylor, The Finite Element Method: Solid Mechanics, Butterworth-Heinemann, 2000.
[8] R. Hill, A self-consistent mechanics of composite materials, J. Mech. Phys. Solids 13 (4) (1965) 213–222.
[9] N. Charalambakis, Homogenization techniques and micromechanics. a survey and perspectives, Appl. Mech. Rev. 63 (3) (2010) 030803.
[10] S. Nemat-Nasser, M. Hori, Micromechanics: Overall Properties of Heterogeneous Materials, Elsevier, Amsterdam, 1999.
[11] E. Cosserat, F. Cosserat, M. Brocato, K. Chatzis, Théorie des Corps Déformables, A. Hermann, Paris, 1909.
[12] N. Fleck, J. Hutchinson, Strain gradient plasticity, Adv. Appl. Mech. 33 (1997) 295–361.
[13] P. Germain, The method of virtual power in continuum mechanics. part 2: Microstructure, SIAM J. Appl. Math. 25 (3) (1973) 556–575.
[14] N. Fleck, G. Muller, M. Ashby, J. Hutchinson, Strain gradient plasticity: Theory and experiment, Acta Metall. Mater. 42 (2) (1994) 475–487.
[15] R. Mindlin, Micro-structure in linear elasticity, Arch. Ration. Mech. Anal. 16 (1) (1964) 51–78.
[16] W.K. Liu, L. Siad, R. Tian, S. Lee, D. Lee, X. Yin, W. Chen, S. Chan, G.B. Olson, L. Lindgen, Complexity science of multiscale materials via stochastic computations, Internat. J. Numer. Methods Engrg. 80 (6-7) (2009) 932–978.
[17] W.K. Liu, C. McVeigh, Predictive multiscale theory for design of heterogeneous materials, Comput. Mech. 42 (2) (2008) 147–170.
[18] Eduardo A. de Souza Neto, D. Peric, D.R.J. Owen, Computational Methods for Plasticity: Theory and Applications, John Wiley & Sons, 2011.
[19] C. Sansour, S. Skatulla, H. Zbib, A formulation for the micromorphic continuum at finite inelastic strains, Int. J. Solids Structures 47 (11) (2010) 1546–1554.
[20] R. Chambon, D. Caillerie, T. Matsuchima, Plastic continuum with microstructure, local second gradient theories for geomaterials: Localization studies, Int. J. Solids Structures 38 (46) (2001) 8503–8527.

[21] T. Belytschko, B. Moran, W.K. Liu, Nonlinear Finite Element Analysis for Continua and Structures, Wiley, 1999.
[22] M.A. Crisfield, Non-linear Finite Element Analysis of Solids and Structures: Advanced Topics, John Wiley & Sons, Inc., 1997.
[23] J.C. Simo, A framework for finite strain elastoplasticity based on maximum plastic dissipation and the multiplicative decomposition. Part II: Computational aspects, Comput. Methods Appl. Mech. Eng. 68 (1) (1988) 1–31.
[24] J. Simo, T. Hughes, Computational inelasticity. 1998, New York.